

## Frictional two-layer exchange flow

By LILLIAN J. ZAREMBA<sup>1</sup>, G. A. LAWRENCE<sup>1</sup>  
AND R. PIETERS<sup>1,2</sup>

<sup>1</sup>Department of Civil Engineering, University of British Columbia, Vancouver,  
BC V6T 1Z4, Canada

<sup>2</sup>Department of Earth and Ocean Sciences, University of British Columbia, Vancouver,  
BC V6T 1Z4, Canada

(Received 2 May 2001 and in revised form 13 August 2002)

A numerical model is developed to study the effects of friction on the steady exchange flow that evolves when a barrier is removed from a constriction separating two reservoirs of slightly different densities. The model has excellent agreement with an analytical solution and laboratory measurements of exchange flows through channels of constant width and depth. The model reveals three viscous flow regimes for a convergent–divergent contraction of constant depth, and three additional viscous flow regimes when an offset sill is introduced. Each regime is characterized by a different set of internal hydraulic control locations. Examination of the predicted interface profiles reveals that it is not possible to distinguish between different flow regimes on the basis of these profiles alone.

---

### 1. Introduction

Two-layer exchange flows often occur when a constriction separates two bodies of water with different densities. The density difference may arise owing to differences in temperature, salinity and/or sediment concentration. Understanding exchange flow is important when addressing water quality issues in semi-enclosed bodies such as harbours, bays, fjords and inlets. A classic example is the exchange of more saline Mediterranean water with Atlantic water through the Strait of Gibraltar (e.g. Armi & Farmer 1988; Farmer & Armi 1988). Important exchange flows occur in other straits including the Bosphorus and Dardanelles which connect the Aegean and Black Seas via the Marmara Sea (Oğuz & Sur 1989; Gregg & Özsoy 2002) and the Bab-el-Mandeb which connects the Indian Ocean to the Red Sea (Murray & Johns 1997). Understanding exchange flow can be important in engineering problems. For example, the design of a bridge linking Denmark and Sweden required zero reduction in exchange flow through the Great Belt between the Baltic and North Seas (Ottesen Hansen & Møller 1990). Another exchange of environmental concern is that of heavily polluted water from Hamilton Harbour with Lake Ontario water through the Burlington Ship Canal (Hamblin & Lawrence 1990).

Many important features of exchange flows can be described by steady hydraulic theory of two-layer inviscid (frictionless) flows (e.g. Armi & Farmer 1986; Farmer & Armi 1986). Maximal exchange occurs when the flow through a strait is isolated from reservoir conditions by supercritical exit regions, requiring the presence of two internal hydraulic controls. Submaximal exchange occurs when one of the controls is lost because of reservoir conditions (Armi & Farmer 1986). In the absence of friction, the flow is relatively easy to predict because controls are generally located

	$L$ (km)	$H$ (m)	$f_b$	$\alpha = f_b L/H$	Source
Bab el Mandeb	160	172	0.012	11.2	Defant (1961)
	160	180	0.03	26.7	Assaf & Hecht (1974)
	160	180	0.012	10.7	Maderich & Efroimson (1990)
Bering Strait	100	50	0.002	4.0	Pratt (1986)
Bosphorus	30	60	0.0046	2.3	Defant (1961)
	30	60	0.03	15.0	Assaf & Hecht (1974)
	20	20	0.002	2.0	Pratt (1986)
	31	40	0.012	9.3	Maderich & Efroimson (1990)
	30	50	0.0046	2.8	Oğuz <i>et al.</i> (1990)
Burlington Ship Canal	0.84	9.5	0.0052	0.4	Dick & Marsalek (1973)
Dardanelles	60	70	0.012	10.3	Defant (1961), Maderich & Efroimson (1990)
	60	70	0.03	25.7	Assaf & Hecht (1974)
	65	55	0.0046	5.4	Oğuz <i>et al.</i> (1990)
Denmark Strait	500	500	0.002	2.0	Pratt (1986)
Ecuador Trench	300	300	0.002	2.0	Pratt (1986)
Gibraltar	60	300	0.012	2.4	Defant (1961)
	60	350	0.03	5.1	Assaf & Hecht (1974)
	20	200	0.002	0.2	Pratt (1986)
	50	300	0.012	2.0	Maderich & Efroimson (1990)
Iceland–Faroe Ridge	400	400	0.002	2.0	Pratt (1986)

TABLE 1. Dimensions and frictional parameters  $f_b$  and  $\alpha$  for various straits. Definitions of  $f_b$  vary; here we have adjusted all values to be consistent with the present paper.

at topographical features such as the crests of sills and the narrowest sections of contractions (Armi & Farmer 1986).

The introduction of friction causes controls to move away from their inviscid positions both in single-layer flow (Henderson 1966; Pratt 1986) and in two-layer flow (Zhu & Lawrence 2000). To avoid the need to determine control locations in advance for a frictional channel, an unsteady model is used in the present study. The control locations are determined by running the unsteady model to steady state.

The effect of friction on two-layer flow was first considered by Schijf & Schönfeld (1953) in their classic study of a salt wedge. Anati, Assaf & Thompson (1977) examined the relative importance of frictional and inertial forces in exchange flows in constant-width channels. They classified the dynamic length of the channel by the parameter  $f_b L/H$ , where  $f_b$  is the bottom drag coefficient,  $L$  is the channel length, and  $H$  is the channel depth. In a short channel,  $f_b L/H \ll 1$  and bottom friction can be neglected compared to inertial forces. In a long channel,  $f_b L/H \gg 1$  and inertial forces can be neglected. In channels of marginal length,  $f_b L/H \approx 1$  and both terms are important. Estimates of  $f_b L/H$  compiled in table 1 indicate that, in general, sea straits are either marginal or long.

The objective of the present study is to investigate the impact of friction on the steady exchange rate and the location of hydraulic control for various channel geometries. The equations of motion and steady hydraulic theory are presented in § 2. The numerical solution technique is outlined in § 3 and verified using the results of previous analytical and laboratory studies of exchange flow in channels of constant width and depth. The effects of friction on exchange through convergent–divergent contractions both with and without an offset sill are examined in § 4. A summary and conclusions are given in § 5.

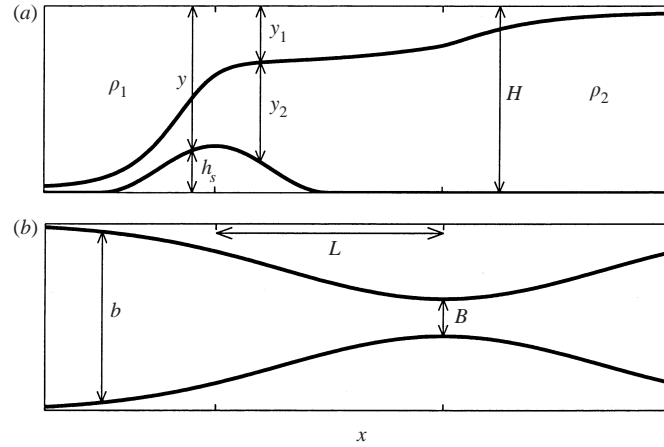


FIGURE 1. Flow configuration for model. (a) Side view of channel with sill. Convention is source of less dense water at left-hand side ( $\rho_1 < \rho_2$ ). During exchange, upper layer flows left to right and lower layer flows right to left. (b) Plan view of convergent-divergent contraction.

## 2. Theory

Consider a system of two layers of homogeneous fluid separated by a sharp interface with variables as defined in figure 1. We extend the approach of Schijf & Schönfeld (1953) by allowing for variations in depth and width. The equations of continuity and momentum in the two layers, neglecting vertical accelerations, are

$$b \frac{\partial y_1}{\partial t} + \frac{\partial}{\partial x} (b y_1 u_1) = 0, \quad (2.1a)$$

$$b \frac{\partial y_2}{\partial t} + \frac{\partial}{\partial x} (b y_2 u_2) = 0, \quad (2.1b)$$

$$\frac{\partial u_1}{\partial t} + \frac{\partial}{\partial x} \left[ \frac{1}{2} u_1^2 + g(y_1 + y_2 + h_s) \right] - g' S_{f_1} = 0, \quad (2.2a)$$

$$\frac{\partial u_2}{\partial t} + \frac{\partial}{\partial x} \left[ \frac{1}{2} u_2^2 + g(y_1(1 - \epsilon) + y_2 + h_s) \right] - g' S_{f_2} = 0, \quad (2.2b)$$

where  $t$  and  $x$  are time and space coordinates, channel width  $b$  and sill height  $h_s$  are given functions of  $x$ , subscript  $i = 1, 2$  indicates upper and lower layers,  $y_i$  and  $u_i$  are layer thickness and velocity,  $\epsilon = (\rho_2 - \rho_1)/\rho_2$  is the relative density difference between the layers where  $\rho_i$  are layer densities, and  $g' = \epsilon g$  is reduced gravity.

The friction slopes for the upper and lower layers, respectively, are given by

$$S_{f_1} = -\frac{1}{2} f_s \frac{u_1 |u_1|}{g' y_1} - f_w \frac{u_1 |u_1|}{g' b} + \frac{1}{2} f_I \frac{\Delta u |\Delta u|}{g' y_1}, \quad (2.3a)$$

$$S_{f_2} = -\frac{1}{2} f_b \frac{u_2 |u_2|}{g' y_2} - f_w \frac{u_2 |u_2|}{g' b} - \frac{1}{2} f_I \frac{\Delta u |\Delta u|}{g' y_2}, \quad (2.3b)$$

where  $\Delta u = u_2 - u_1$  is the shear. The friction factors  $f$  are defined by the shear stresses  $\tau$  on the bottom, surface, sidewalls and interface, respectively:

$$f_b = -2\tau_b/(\rho_2 u_2 |u_2|), \quad f_s = -2\tau_s/(\rho_1 u_1 |u_1|), \quad (2.4a, b)$$

$$f_w = -2\tau_w/(\rho_i u_i |u_i|), \quad f_I = 2\tau_I/(\rho_i \Delta u |\Delta u|). \quad (2.4c, d)$$

To facilitate the investigation of frictional effects, the following simplifications are

made. The density difference between layers is sufficiently small that the Boussinesq approximation  $\rho_1 \approx \rho_2$  applies, so that the friction factors  $f_w$  and  $f_I$  are the same for each layer and free-surface deflections are small. Zero barotropic forcing is assumed so that the transport in each layer is equal. The equation for momentum in the upper layer is subtracted from that in the lower layer, (2.2b)–(2.2a), and we non-dimensionalize  $x$  by length scale  $L$ ,  $y_i$  and  $y$  by depth scale  $H$ ,  $b$  by width scale  $B$ ,  $u_i$  and  $\Delta u$  by  $(g'H)^{1/2}$ , and  $t$  by  $L/(g'H)^{1/2}$ . These simplifications yield the following four equations in the four unknowns  $u_1, u_2, y_1$  and  $y_2$ .

$$y_1 + y_2 + h_s = 1, \quad (2.5)$$

$$y_1 u_1 + y_2 u_2 = 0, \quad (2.6)$$

$$\frac{\partial y_1}{\partial t} + \frac{1}{b} \frac{\partial}{\partial x} (u_1 y_1 b) = 0 \quad (2.7)$$

$$\frac{\partial \Delta u}{\partial t} + \frac{\partial E_I}{\partial x} - S_f = 0, \quad (2.8)$$

where the internal energy is

$$E_I = h_s + y_2 + \frac{1}{2}(u_2^2 - u_1^2), \quad (2.9)$$

and the friction slope is

$$S_f = -\alpha \left\{ \frac{u_2 |u_2|}{2y_2} - r_s \frac{u_1 |u_1|}{2y_1} + r_I \frac{y \Delta u |\Delta u|}{2y_1 y_2} + r_w \frac{u_2 |u_2| - u_1 |u_1|}{b} \right\}. \quad (2.10)$$

The non-dimensionalization has introduced the parameter

$$\alpha = f_b \frac{L}{H}, \quad (2.11)$$

which is the ratio of bottom friction to inertia introduced by Anati *et al.* (1977). Additional friction ratios have been introduced in (2.10):

$$r_I = \frac{f_I}{f_b}, \quad r_s = \frac{f_s}{f_b}, \quad r_w = \frac{f_w H}{f_b B}. \quad (2.12)$$

Each exchange flow is prescribed by the geometry of the channel, the density difference across the channel, and the four frictional parameters  $\alpha$ ,  $r_I$ ,  $r_s$  and  $r_w$ .

### 2.1. Steady hydraulics

Armi (1986) has shown that the status of a steady two-layer flow is given by the composite Froude number

$$G^2 = F_1^2 + F_2^2 - \epsilon F_1^2 F_2^2, \quad (2.13)$$

where the layer Froude numbers are  $F_i^2 = u_i^2 / y_i$  with  $u_i$  and  $y_i$  non-dimensionalized as above. In the present study, the density difference between layers is small ( $\epsilon \ll 1$ ) and the last term in (2.13) is ignored. Interfacial waves cannot propagate out of regions of supercritical flow ( $G^2 > 1$ ), thus if flow in a channel is bounded by two controls with supercritical flow beyond, flow is isolated from reservoir conditions. This is known as maximal exchange (Armi & Farmer 1986). The above discussion presumes that long interfacial waves are stable to small disturbances. The stability of long internal waves is determined by the stability Froude number

$$F_\Delta^2 = \frac{(\Delta u)^2}{y_1 + y_2}. \quad (2.14)$$

Long waves are stable for  $F_\Delta^2 \leq 1$ . When  $F_\Delta^2 > 1$ , internal phase speeds are imaginary and internal hydraulics may no longer apply (Long 1954; Lawrence 1990).

Consider the steady solution of (2.8). For the inviscid case, internal energy is conserved along a channel in the absence of hydraulic jumps. When friction is included, shear stresses at the bottom, sidewalls, interface and surface result in energy losses, i.e.  $dE_I/dx = S_f$ . Substituting the equation for internal energy head, (2.9), into the steady form of (2.8), we obtain an expression for the slope of the interface

$$\frac{dy_1}{dx} = \frac{S_o - S_f}{1 - G^2}, \quad (2.15)$$

where

$$S_o = \frac{u_2^2}{y_2} \frac{dh_s}{dx} - \frac{u_2^2 - u_1^2}{b} \frac{db}{dx}, \quad (2.16)$$

is the topographic slope due to changes in depth and width. The flow is subject to hydraulic controls where the composite Froude number is unity,  $G^2 = 1$ . At these points, the topographic slope must equal the friction slope, i.e.  $S_o = S_f$ , as in single-layer flow (Henderson 1966; Pratt 1986).

### 3. Solution technique

The present study focuses on effects of friction on the steady exchange flow that evolves after a barrier is removed from a constriction separating two reservoirs of slightly different density. In the absence of friction, steady solutions can be obtained directly if the locations of hydraulic control are known. Armi & Farmer (1986) and Farmer & Armi (1986) have derived inviscid solutions for simple geometries (contraction, sill, and combination of contraction and sill). With the addition of friction or with a complicated geometry, it is necessary to model the unsteady evolution of the flow until steady state is achieved.

Inviscid, unsteady exchange flow was investigated by Helfrich (1995) who rearranged (2.5) and (2.6) to obtain

$$u_1 = \frac{-\Delta u(y - y_1)}{y}, \quad u_2 = \frac{\Delta u y_1}{y}, \quad (3.1a, b)$$

which allows (2.7) and (2.8) to be written in terms of the variables  $y_1$  and  $\Delta u$ , i.e.:

$$\frac{\partial y_1}{\partial t} + \frac{1}{b} \frac{\partial}{\partial x} \left\{ \Delta u b y_1 \left( \frac{y_1}{y} - 1 \right) \right\} = 0, \quad (3.2)$$

$$\frac{\partial \Delta u}{\partial t} + \frac{\partial}{\partial x} \left\{ (\Delta u)^2 \left( \frac{y_1}{y} - \frac{1}{2} \right) - y_1 \right\} - S_f = 0. \quad (3.3)$$

Equations (3.2) and (3.3) are solved numerically using the two-step Lax–Wendroff method as outlined in Press *et al.* (1986). The method has second-order accuracy in time and space. It is able to model the development and propagation of shocks (internal hydraulic jumps) which can occur in exchange flows. Sommerfeld radiation boundary conditions (Orlanski 1976) are applied at each end of the strait so that information propagates out of the domain. In some cases, the inclusion of numerical dissipation was required to control the growth of numerical instabilities at internal hydraulic jumps. As in Helfrich (1995), the term  $\nu(\Delta u)_{,xx}$  was added to the right-hand side of (3.3). Numerical viscosities of  $\nu \leq 10^{-3}$  were sufficient to ensure stability, without noticeably affecting the solutions.

	$L$ (cm)	$H$ (cm)	$B$ (cm)	$W$ (cm)	$g'$ (cm s <sup>-2</sup> )	$f_b$	$\alpha$	$r_I$	$r_s$	$r_w$
Gu (2001)	200	28	15.2	106	1.14	0.0104	0.074	0.375	0.0	1.8
Anati <i>et al.</i> (1977)	60	7.75	1.0	16	0.015	0.12	0.92	0.1	0.0	7.75

TABLE 2. Parameters from laboratory experiments of Anati *et al.* (1977) and Gu (2001).

The model was typically initiated as a lock exchange problem, mimicking the removal of a vertical barrier in a channel. The exchange flow is established by gravity currents which travel out from the centre of the strait. Once they reach the ends of the channel, the gravity heads are swept out of the model domain by the open boundary, establishing the steady-state solution. The choice of initial conditions did not affect the final steady solution. The solution was considered steady when the variation in time of the interface position became sufficiently small, i.e.  $y_1(t + \Delta t) - y_1(t) \leq 10^{-8}$ , where  $\Delta t$  is the model time step.

### 3.1. Model verification

The problem of exchange through a channel of constant width and depth opening into reservoirs via sudden expansions, as depicted in figure 2(a), has attracted the attention of a number of investigators. In this section, we compare the results of our numerical model with the theoretical analyses and laboratory experiments of Anati *et al.* (1977) and Gu (2001). The dimensions and frictional parameters for the laboratory experiments are given in table 2. Gu's (2001) laboratory flow was turbulent, and  $f_b$  was determined using the method of Thwaites (1949). The laboratory flow of Anati *et al.* (1977) was laminar and we set  $f_b = 16/Re$ . In both cases, we set  $f_w = f_b$  so that  $r_w = H/B$ . We estimate  $f_I$  indirectly by fitting (2.8)–(2.10) to the experimental data (see Zhu & Lawrence 2000).

Gu (2001) developed an analytical solution for exchange rate and interface position by direct integration of the fully nonlinear hydraulic equation, assuming controls at either end of the channel. His analytical solution is indistinguishable from our numerical solution. Both the analytical and numerical solutions agree extremely well with Gu's (2001) laboratory experiment (figure 2b, c). Anati *et al.* (1977) did not determine the precise interface profile analytically, but assumed a linear variation between the hydraulic controls at either end of the channel (figure 2d). For large portions of the strait, this predicted interface position and the corresponding composite Froude number differ from the measured values by an amount greater than can be attributed to experimental error. Our numerical solution matches the experimental data of Anati *et al.* (1977) extremely well (figure 2d, e).

The presence of sudden expansions at the ends of the channels provided a rigorous test of the effectiveness of our solution technique. We can now tackle other geometrical configurations with confidence.

## 4. Frictional exchange through channels of varying cross-section

To demonstrate some of the important effects of friction on exchange flows we model exchange flow through a convergent–divergent contraction (figure 1). The additional flow regimes caused by the presence of friction will be examined. An offset sill is then introduced, resulting in further flow regimes. Together these results reveal

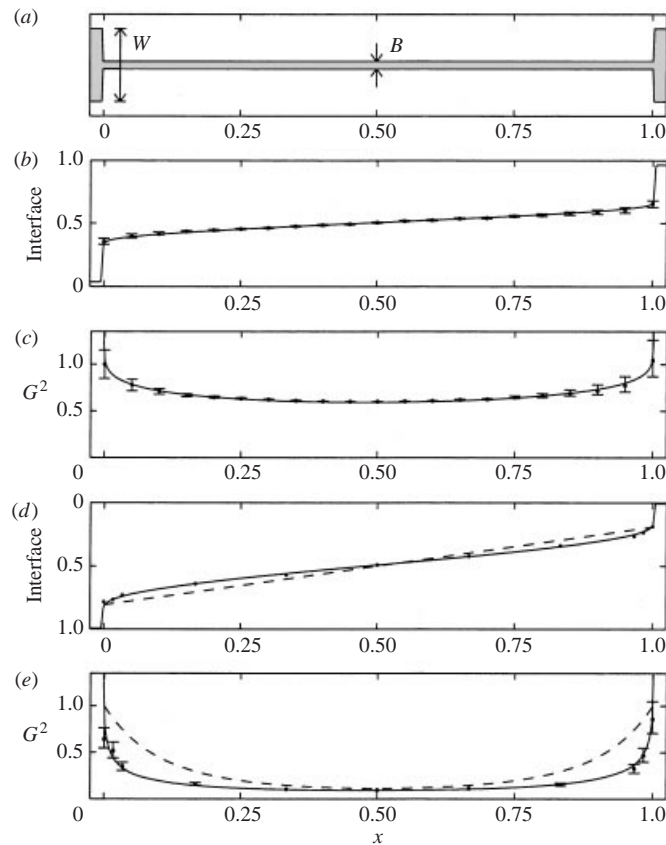


FIGURE 2. Comparison of present model to the analytical and experimental results of Gu (2001) and Anati *et al.* (1977). (a) Plan view of channel. (b) Interface and (c) composite Froude number from  $\bullet$ , laboratory experiment of Gu (2001) and —, from present model. The results of the present model are indistinguishable from Gu's (2001) analytical solution. (d) Interface and (e) composite Froude number from  $\bullet$ , laboratory experiment and ---, analytical solution of Anati *et al.* (1977) and —, from present model. See table 2 for experimental parameters.

the sorts of behaviour that can be expected in the more complicated geometries of natural flows.

A wide range of values of the friction parameter  $\alpha$  are investigated to cover all flow regimes. For the most part, the friction ratios are set at physically realistic values, i.e.  $r_s = 0$ ,  $r_w = 0.1$  and  $r_I = 0.1$ . Unless otherwise stated, these values will be used. There are two exceptions. The first is that we start by setting  $r_s = 1$  because of the symmetries associated with this case. Secondly, we investigate the impact of varying  $r_I$ , since the interfacial friction factor is not an easy parameter to determine in nature (Zhu & Lawrence 2000).

#### 4.1. Convergent–divergent contraction of constant depth

The convergent–divergent contraction (figure 1) has a form similar to that investigated in the inviscid study of Helfrich (1995). The channel width is defined as

$$b = 1 + 4(1 - \exp(-x^2)). \quad (4.1)$$

The effect of friction on the flow through the contraction was investigated by increasing the parameter  $\alpha$ . In the initial analysis, the surface friction ratio was set

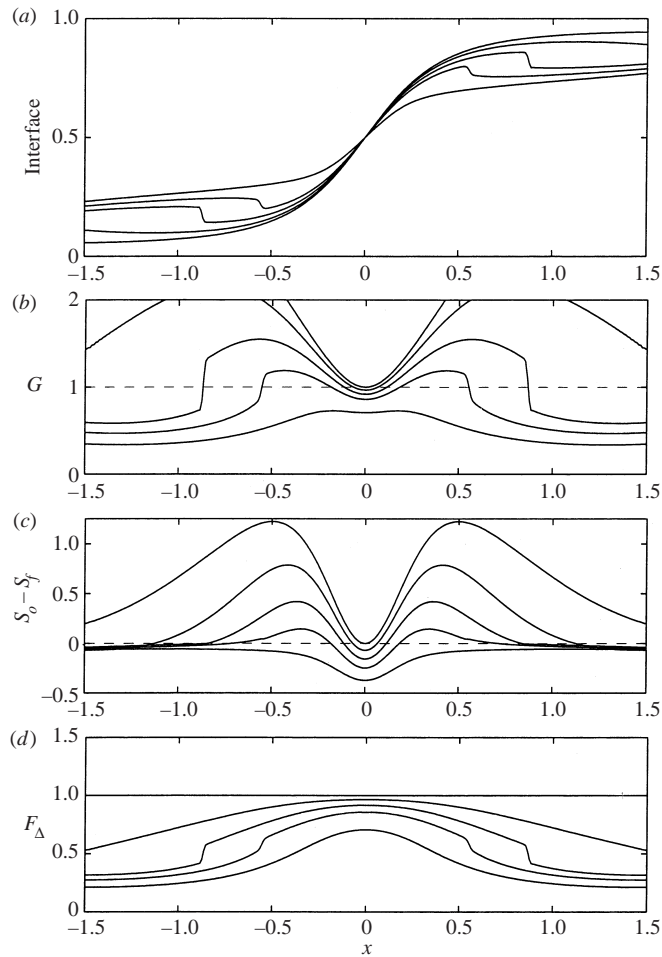


FIGURE 3. Steady solution for contraction with increasing friction. (a) Interface position along canal. (b) Composite Froude number. (c) Topographical slope minus friction slope. (d) Stability Froude number.  $\alpha = 0, 0.1, 0.25, 0.5$  and  $1.0$  from top to bottom in each panel (right-hand side in a). Friction ratios are  $r_s = 1$ ,  $r_I = 0.1$  and  $r_w = 0.1$ .

equal to one ( $r_s = 1$ ) and the interfacial and wall friction ratios were set at  $r_I = 0.1$  and  $r_w = 0.1$ . The results for  $\alpha = 0, 0.1, 0.25, 0.5$  and  $1$  are illustrated in figure 3.

Setting  $r_s = 1$  yields some interesting and instructive results. The interface profiles are anti-symmetric about the narrowest point (narrows) of the contraction (figure 3a). At the narrows, the two layers are of equal thickness ( $y_1 = y_2 = 0.5$ ) and equal velocity ( $|u_1| = |u_2|$ ), so that  $|\Delta u| = 2|u_i|$ . In addition,  $b = 1$  at the narrows so the layer flow  $Q_i = u_i y_i$ . Furthermore, since  $y_i = 0.5$  and  $\Delta u = 2u_i$ ,  $Q_i = \frac{1}{4}\Delta u$  and  $G = F_\Delta = |\Delta u|$ . For inviscid flow,  $G = 1$  at the narrows, so  $\Delta u = 1$  and the inviscid exchange rate  $Q_{inv} = 0.25$ . If the flow is viscous,  $|\Delta u|$  is reduced and  $Q_i/Q_{inv} = G = F_\Delta = |\Delta u| < 1$  at the narrows.

With increasing  $\alpha$ , the nature of the flow varies progressively (figure 3). For the inviscid solution the flow is controlled at the narrows with supercritical flow everywhere else in the strait (figure 3b). Once friction is introduced, two controls form equidistant from the centre of the contraction. At the same time, hydraulic jumps move inward from the ends of the strait (figure 3a). The value of  $\alpha$  when the jumps first appear is



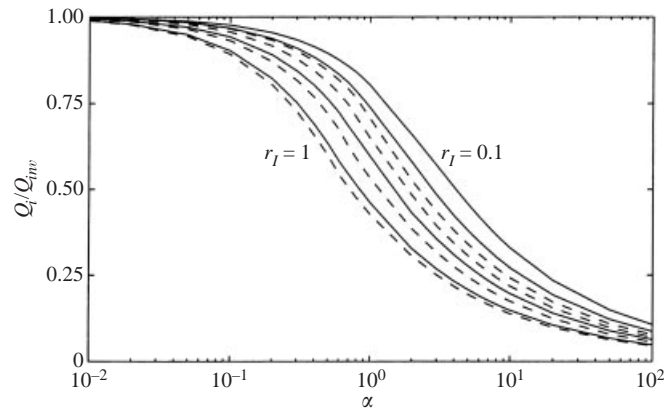


FIGURE 4. Effect of varying friction ratios on exchange through convergent–divergent contraction. Friction ratio for wall is held constant at  $r_w = 0.1$ . Exchange is measured by layer flow  $Q_i$  normalized by the inviscid value  $Q_{inv} = 0.25$ . Interfacial friction decreases from left to right ( $r_I = 1$ ,  $r_I = 0.5$ ,  $r_I = 0.2$ ,  $r_I = 0.1$ ), with surface friction factor equal to bottom friction factor (---,  $r_s = 1$ ) and with zero surface friction (—,  $r_s = 0$ ).

a function of domain length. With the jumps present, the flow is subcritical beyond the jumps as well as in the centre between the two controls, with supercritical regions between the controls and the jumps (figure 3*b*). Although flow is reduced compared to the inviscid solution, this flow is still the maximal exchange for the specified friction parameters, as flow in the channel is isolated from outside conditions by supercritical regions.

The region of supercritical flow between the jumps and controls shrinks as  $\alpha$  increases, until it disappears at  $\alpha = 0.62$ . When  $\alpha > 0.62$ , the jumps and controls disappear and the flow is subcritical everywhere (figure 3*b*). Thus, in addition to the inviscid regime where flow is controlled at the centre with supercritical flow everywhere else, there are two viscous flow regimes. When  $0 < \alpha < 0.62$ , the flow has two sets of internal hydraulic controls and jumps. When  $\alpha > 0.62$ , the flow is subcritical everywhere.

The nature of the flow regimes is further illustrated by plotting  $S_o - S_f$  (figure 3*c*). Recall from (2.15) that  $S_o - S_f = 0$  at points of control. Note from (2.16) that for the geometry we are considering  $S_o$  is always positive, except at the narrows where  $S_o = 0$ , since  $u_2 = -u_1$  there. From (2.10),  $S_f = 0$  when  $\alpha = 0$ , otherwise  $S_f > 0$ . Thus, when  $\alpha = 0$ ,  $S_o - S_f = 0$  at the narrows where  $G = 1$ , and  $S_o - S_f > 0$  everywhere else where the flow is supercritical. For  $0 < \alpha < 0.62$ , the  $S_o - S_f$  curves are lowered, since  $S_f > 0$ , and there are at least two pairs of points where  $S_o - S_f = 0$ . The pairs nearest the narrows are the controls and the more distant pairs correspond to the point where  $dy_1/dx = 0$  while  $G \neq 1$  (see (2.15)). For  $\alpha > 0.62$ ,  $S_o - S_f < 0$  everywhere and the flow is subcritical everywhere.

For all positive  $\alpha$ , the flow is stable along the channel ( $F_\Delta < 1$ ). The stability Froude number is highest at the narrows. As friction increases, the maximum value of  $F_\Delta$  decreases (figure 3*d*). The layer flow rate of the steady solution similarly decreases from its inviscid value of  $Q_{inv} = 0.25$  with increasing friction (figure 4). The reduction cannot be neglected even if  $\alpha$  is as low as 0.1.

#### 4.1.1. Varying friction ratios

It is of practical importance to investigate the effects of setting  $r_s = 0$  rather than  $r_s = 1$ , and to vary  $r_I$ . When  $r_s = 0$ , the solution is no longer symmetric along

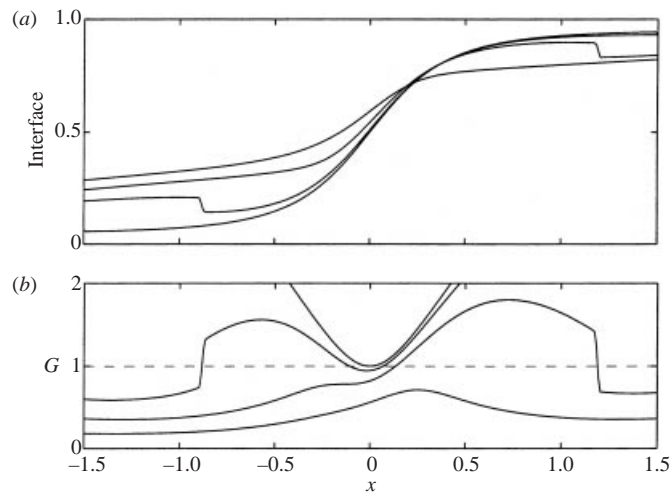


FIGURE 5. Steady solution for contraction with zero surface friction. (a) Interface position along canal. (b) Composite Froude number.  $\alpha = 0, 0.25, 1$  and  $4$  from top to bottom in each panel (right-hand side in a). Friction ratios are  $r_s = 0$ ,  $r_l = 0.1$  and  $r_w = 0.1$ .

the canal. The upper layer is less constrained resulting in higher composite Froude numbers, particularly in the right-hand portion of the contraction. The effects of varying  $\alpha$  with  $r_s = 0$  are shown in figure 5. As in the case when  $r_s = 1$ , the controls move out from the centre with increasing friction. Hydraulic jumps move in from the ends of the canal with increasing friction, appearing at the left-hand side first (figure 5a). The left-hand control is drowned for  $\alpha > 0.65$ ; flow is now subcritical except for the region between the right-hand control and the right-hand hydraulic jump. Flow becomes uncontrolled when  $\alpha > 2.8$ , with subcritical flow throughout (figure 5b).

Varying  $r_l$  does not change the basic features of the flow regimes, but it does change the values of  $\alpha$  at which transitions between regimes occur. We can classify the regimes of viscous flow for varying  $\alpha$  and  $r_l$  according to the number of controls (figure 6). When  $r_s = 1$ , two viscous regimes are possible: a regime characterized by a control on either side of the narrows; and an uncontrolled regime. In the absence of surface friction, three regimes are observed: a regime with controls on either side of the narrows; a regime with a control to the right of the narrows; and an uncontrolled regime. The curve separating the two-control and no-control regimes for  $r_s = 1$  is very close to that separating the two-control and one-control regimes for  $r_s = 0$ . As interfacial friction ratio  $r_l$  increases, the transition to uncontrolled flow occurs at lower  $\alpha$  for both  $r_s = 1$  and  $r_s = 0$ .

The effect of changing friction ratios on exchange rate is shown in figure 4. The results are consistent with what we would expect. In all cases increasing any one of  $\alpha$ ,  $r_l$  or  $r_s$  while holding the others constant results in a reduction of the exchange rate. It is worth noting that  $\alpha$  must be substantially less than unity before friction can be ignored.

The friction ratios contribute to the friction slope  $S_f$ , (2.10), with varying degrees of importance. Most natural channels are wide, so the aspect ratio is small ( $H/B \ll 1$ ). The wall friction ratio is thus small ( $r_w \ll 1$ ), so it does not affect exchange greatly. Changing surface friction has an impact on the flow primarily where the upper layer is active (i.e. where it is thinner) whereas the interfacial friction acts on both layers.

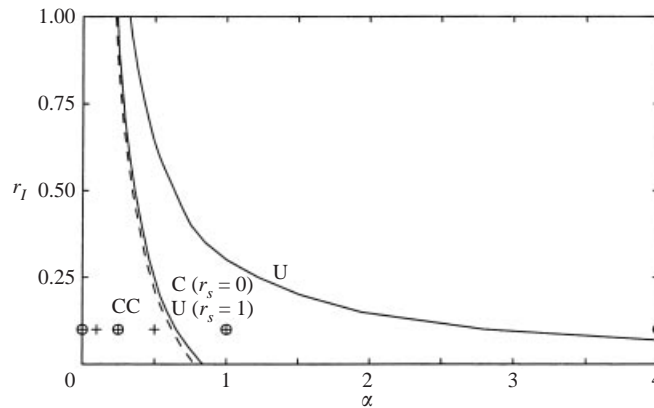


FIGURE 6. Classification diagram for contraction. When  $\alpha = 0$  (inviscid flow) there is one control at the narrowest point of the contraction. For  $\alpha > 0$  and  $---$ ,  $r_s = 1$ , two controls are present to the left of the dashed line (CC) and flow is uncontrolled to the right of the dashed line (U). For zero surface friction ( $-$ ,  $r_s = 0$ ), three regimes are possible: CC, two controls; C, one control; U, uncontrolled. Wall friction ratio is  $r_w = 0.1$  for all cases. +, values of  $\alpha$  for which solutions are plotted in figure 3 and  $\circ$  in figure 5.

Interfacial friction is proportional to the square of the shear  $(\Delta u)^2$  while the other friction terms are proportional to the square of layer velocities  $u_i^2$ . Thus, the exchange rate is sensitive to variations in  $r_I$ , which is of practical importance since it is difficult to estimate the interfacial friction factor accurately.

#### 4.2. Convergent-divergent contraction with offset sill

A sill offset from the narrows with its midpoint at  $x = -1$  and with topography given by

$$h_s(x) = H_s \cos\{\pi(x+1)\}^2 \quad \text{for } |x+1| \leq 0.5, \quad (4.2)$$

was tested with varying crest heights  $H_s$ . The effect of friction on the solution was examined by varying  $\alpha$  while holding the friction ratios constant at  $r_s = 0$ ,  $r_I = 0.1$  and  $r_w = 0.1$ . As expected, the exchange rate decreases with increasing  $\alpha$  and with increasing  $H_s$  (figure 7). Somewhat less expected is the large number of flow regimes that are revealed when  $H_s$  and  $\alpha$  are varied. Each regime is characterized by a different set of internal hydraulic control locations (figure 8). Six regimes are possible: SCC (control at sill and two controls in contraction); SC (control at sill and single control in contraction); S (control at sill); CC (two controls in contraction); C (single control in contraction); and U (uncontrolled). The classification diagram that specifies the regime of flow given  $\alpha$  and  $H_s$  is complex (figure 8). We will illustrate the nature of each regime by examining sills of height  $H_s = 0.6$  and  $H_s = 0.1$ .

The variation in interface position, composite and stability Froude numbers for various values of  $\alpha$  for a sill of height  $H_s = 0.6$  are presented in figure 9. Single controls are present at the crest of the sill and the narrowest point of the contraction (regime SC) when flow is inviscid (figure 9*b*). Flow is subcritical between the controls and supercritical beyond. As  $\alpha$  increases, the controls move outward while hydraulic jumps move inward. The control at the contraction is lost first (regime S). Eventually, the control at the sill is lost and the flow becomes subcritical throughout (regime U).

Note that the interface profiles are almost identical irrespective of the regime of flow or the value of  $\alpha$  (figure 9*a*). The inviscid case is the exception in that the flow becomes very thin on the left-hand side of the sill. In fact, it becomes so thin that  $F_\Delta > 1$

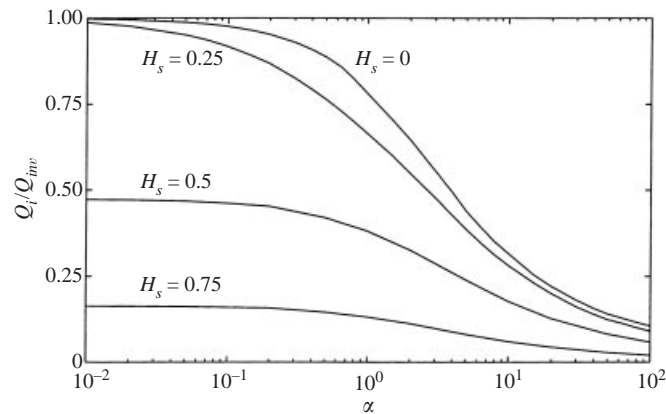


FIGURE 7. Reduction of exchange with friction in contraction with offset sill of varying height. Friction ratios are  $r_s = 0$ ,  $r_l = 0.1$  and  $r_w = 0.1$ .

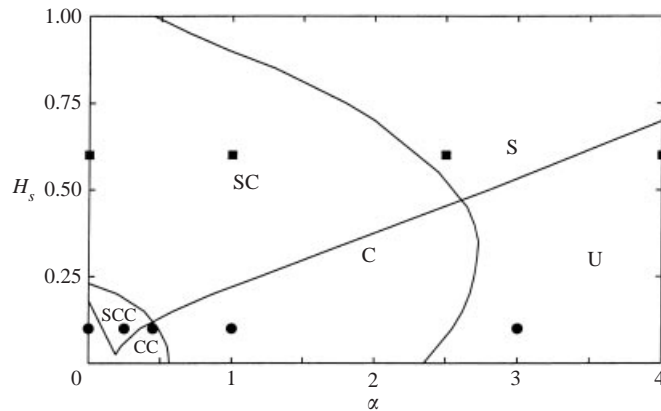


FIGURE 8. Classification diagram for contraction with offset sill of varying height  $H_s$ . Friction ratios are  $r_s = 0$ ,  $r_l = 0.1$  and  $r_w = 0.1$ . Regimes are: SC, control at sill and one control in contraction; S, control at sill; U, uncontrolled; SCC, control at sill and two controls in contraction; CC, two controls in contraction; C, one control in contraction. ■, values of  $\alpha$  for which solutions are plotted in figure 9 and ●, in figure 10.

(figure 9c), indicating intense interfacial mixing that would thicken the lower layer. There is a little more variation in the interface profiles for the other cases investigated (see figures 3, 5 and 10). However, in all cases there exist different regimes of flow with qualitatively very similar interface profiles. Furthermore, in natural flows which are subject to more complicated geometry, continuous stratification and unsteady forcing, any differences are likely to be masked or difficult to interpret. Thus, the interface profile is a poor indicator of the regime of flow. A similar result was obtained by Pratt (1986) for frictional single-layer flow over a sill.

The progression of regimes is shown for a sill of height  $H_s = 0.1$  in figure 10. For inviscid flow, there is a control at the narrows and the flow is supercritical everywhere else. For very low values of  $\alpha$ , controls appear on either side of the narrows (regime CC). As  $\alpha$  is increased, a control appears at the sill (regime SCC). The sill control is only present over a narrow range of  $\alpha$ , after which the flow reverts to regime CC again. At slightly higher  $\alpha$ , the left-hand control is lost, so that just one control

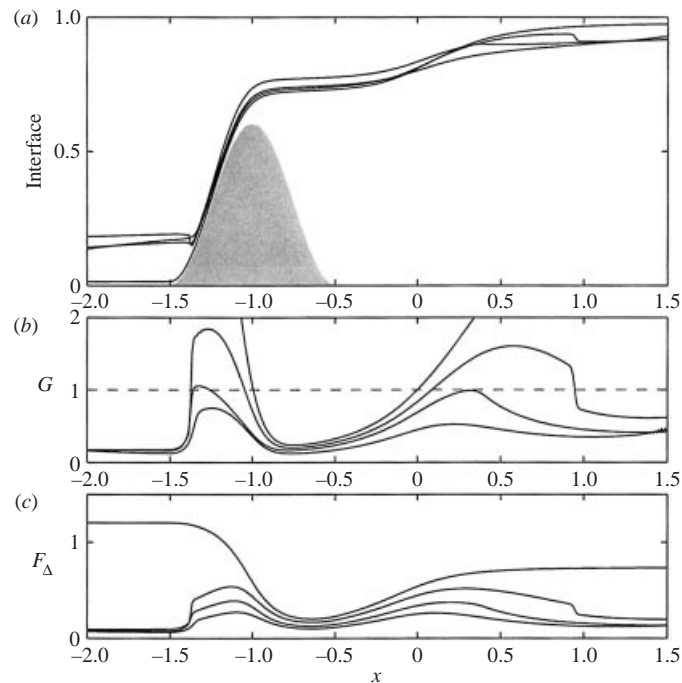


FIGURE 9. Effect of varying friction on steady solution, for contraction (at  $x = 0$ ) with offset sill (at  $x = -1$ ) of height  $H_s = 0.6$ . (a) Interface position along canal. (b) Composite Froude number. (c) Stability Froude number.  $\alpha = 0, 1, 2.5$  and  $4$  from top to bottom in each panel (right-hand side in a). Friction ratios are  $r_s = 0$ ,  $r_l = 0.1$  and  $r_w = 0.1$ .

remains, located on the right-hand side of the contraction (regime C). Note that there are three regime transitions for  $\alpha < 0.5$ . Eventually ( $\alpha > 2.55$ ), the flow becomes uncontrolled (regime U).

The various flow regimes described above result from the competing influences of changes in depth and width. The values of  $\alpha$  at which transitions occur are specific to the particular geometry considered and would change with varying curvature of the sill or the contraction, or location of the sill with respect to the narrows of the contraction. The transitional values of  $\alpha$  depend on the values of the friction ratios. Additional sills and contractions would add to the number of possible control locations and the number of flow regimes. Such refinements, although of potential practical significance, would probably not add to our basic understanding, and are beyond the scope of the present study.

## 5. Summary and conclusions

An unsteady, one-dimensional model of frictional two-layer exchange flow through a strait was developed. Friction can be applied to the bottom, sidewalls, surface and interface of the channel. The frictional parameters are

$$\alpha = f_b \frac{L}{H}, \quad r_l = \frac{f_l}{f_b}, \quad r_s = \frac{f_s}{f_b}, \quad r_w = \frac{f_w H}{f_b B}, \quad (5.1)$$

where  $\alpha$  is the ratio of frictional to inertial forces and  $r_l$ ,  $r_s$  and  $r_w$  are the friction ratios for the interface, surface and sidewalls, respectively. To solve the model equations,

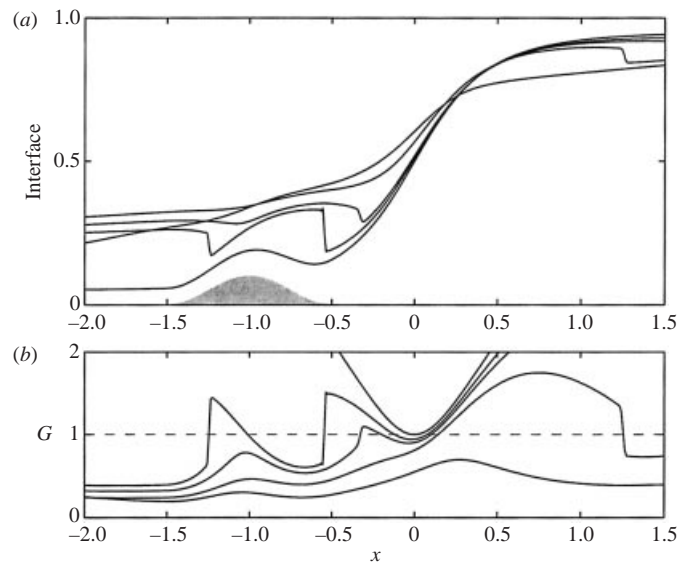


FIGURE 10. Effect of varying friction on steady solution, for contraction (at  $x = 0$ ) with offset sill (at  $x = -1$ ) of height  $H_s = 0.1$ . (a) Interface position along canal. (b) Composite Froude number.  $\alpha = 0, 0.25, 0.45, 1$  and  $3$  from top to bottom in each panel (right-hand side in a). Friction ratios are  $r_s = 0$ ,  $r_I = 0.1$  and  $r_w = 0.1$ .

the channel geometry must be specified in addition to these parameters. Width and depth can vary along the channel. The model was applied to a contraction with an offset sill of varying height and to a constant-width channel with abrupt expansions and constant depth. The effect of friction on the interface position, Froude numbers and layer flows was investigated.

The model was solved numerically for the unforced steady solution by running a lock exchange until steady state was reached. The unsteady model is useful for finding the steady solution when it is difficult to predict control locations in channels with friction and/or complex geometry. Model results compared well with laboratory studies and with Gu's (2001) analytical solution of steady exchange flow through a constant-width channel.

The impact of friction on steady exchange rate is similar for all geometries studied (figures 4 and 7). The layer flow rate decreases from the inviscid value with increasing friction. The exchange is reduced by up to a half for a contraction of marginal length ( $\alpha = 1$ ). Even for short contractions ( $\alpha \ll 1$ ), flow is reduced substantially from the inviscid prediction. For a contraction with an offset sill, three changes of flow regime can occur for  $\alpha < 0.5$ . This result is of practical importance since most natural sea straits are dynamically long or marginal (table 1). Thus, the applicability of inviscid theory in predicting flow in sea straits is limited.

Traditionally, studies of two-layer exchange flow have assumed that flow is governed by controls at topographical features such as a sudden expansion in width, the narrowest point of a contraction, and the crest of a sill. Friction changes the location of controls. With increasing friction, controls at topographical features move outward while internal hydraulic jumps move inward from the ends of the channel. The controls are lost when they merge with the internal hydraulic jumps. For contractions with offset sill, six viscous regimes of flow are possible in addition to the inviscid regimes. The transitions between regimes occur over a wide range of  $\alpha$ .

Uncontrolled flow occurs when  $\alpha$  is sufficiently high. The different regimes cannot reliably be distinguished from each other on the basis of the interfacial profiles alone.

Financial assistance from the Natural Sciences and Engineering Research Council of Canada is gratefully acknowledged. G. A. L. is also grateful for the support of a Canada Research Chair. Karl Helfrich kindly provided us with a copy of his inviscid numerical model.

## REFERENCES

- ANATI, D., ASSAF, G. & THOMPSON, R. 1977 Laboratory models of sea straits. *J. Fluid Mech.* **81**, 341–351.
- ARMI, L. 1986 The hydraulics of two flowing layers with different densities. *J. Fluid Mech.* **163**, 27–58.
- ARMI, L. & FARMER, D. 1986 Maximal two-layer exchange flow through a contraction with barotropic net flow. *J. Fluid Mech.* **164**, 27–51.
- ARMI, L. & FARMER, D. M. 1988 The flow of Mediterranean water through the Strait of Gibraltar. *Progr. Oceanogr.* **21**, 1–105.
- ASSAF, G. & HECHT, A. 1974 Sea straits: a dynamical model. *Deep-Sea Res.* **21**, 947–958.
- DEFANT, A. 1961 *Physical Oceanography*, vol. 1. Pergamon.
- DICK, T. & MARSALEK, J. 1973 Exchange flow between Lake Ontario and Hamilton Harbour. In *Environment Canada Inland Waters Directorate, Scientific Series No. 36*.
- FARMER, D. & ARMI, L. 1986 Maximal two-layer exchange over a sill and through the combination of a sill and contraction with barotropic flow. *J. Fluid Mech.* **164**, 53–76.
- FARMER, D. & ARMI, L. 1988 The flow of Atlantic water through the Strait of Gibraltar. *Progr. Oceanogr.* **21**, 1–105.
- GREGG, M. & ÖZSOY, E. 2002 Flow, water mass changes, and hydraulics in the Bosphorus. *J. Geophys. Res.* **107** (C3), 10.1029/2000JC000485.
- GU, L. 2001 Frictional exchange flow through a wide channel with application to the Burlington Ship Canal. PhD thesis, Dept of Civil Engineering, University of British Columbia.
- HAMBLIN, P. & LAWRENCE, G. 1990 Exchange flows between Hamilton Harbour and Lake Ontario. In *Proc. 1st Biennial Environmental Specialty Conference, CSCE*, pp. 140–148.
- HELFRICH, K. R. 1995 Time-dependent two-layer hydraulic exchange flows. *J. Phys. Oceanogr.* **25**, 359–373.
- HENDERSON, F. M. 1966 *Open Channel Flow*. Macmillan.
- LAWRENCE, G. 1990 On the hydraulics of Boussinesq and non-Boussinesq two-layer flows. *J. Fluid Mech.* **215**, 457–480.
- LONG, R. R. 1954 Some aspects of the flow of stratified fluids II: experiments with two fluids. *Tellus* **6**, 97–115.
- MADERICH, V. S. & EFROMSON, V. 1990 Theory for water exchange across a strait. *Oceanology* **30**, 415–420.
- MURRAY, S. & JOHNS, W. 1997 Direct observations of seasonal exchange through the Bab el Mandab Strait. *Geophys. Res. Lett.* **24**, 2557–2560.
- OĞUZ, T., ÖZSOY, E., LATIF, M., SUR, H. & ÜNLÜATA, U. 1990 Modeling of hydraulically controlled exchange flow in the Bosphorus Strait. *J. Phys. Oceanogr.* **20**, 945–965.
- OĞUZ, T. & SUR, H. 1989 A two-layer model of water exchange through the Dardanelles Strait. *Oceanol. Acta* **12**, 23–31.
- ORLANSKI, I. 1976 A simple boundary condition for unbounded hyperbolic flows. *J. Comput. Phys.* **21**, 251–269.
- OTTESEN HANSEN, N. & MØLLER, J. 1990 Zero blocking solution for the Great Belt Link. In *The Physical Oceanography of Sea Straits* (ed. L. Pratt), pp. 153–170. Kluwer.
- PRATT, L. 1986 Hydraulic control of sill flow with bottom friction. *J. Phys. Oceanogr.* **16**, 1970–1980.
- PRESS, W., FLANNERY, B., TEUKOLSKY, S. & VETTERLING, W. 1986 *Numerical Recipes*. Cambridge University Press.

- SCHIJF, J. & SCHÖNFELD, J. 1953 Theoretical considerations on the motion of salt and fresh water. In *Proc. of the Minn. Intl Hydraulics Conv.* Joint meeting IAHR and Hyd. Div., ASCE, pp. 321–333.
- THWAITES, B. 1949 Approximate calculation of the laminar boundary layer. *Aeronaut. Q.* **1**, 245–280.
- ZHU, D. Z. & LAWRENCE, G. 2000 Hydraulics of exchange flows. *J. Hydr. Engng. ASCE* **126**, 921–928.